Molecular Neurobiology

ISSN0893-7648/03/28(2):139–147/$25.00

Retinal Remodeling in Inherited Photoreceptor Degenerations

Robert E. Marc* and Bryan W. Jones

John A. Moran Eye Center, University of Utah School of Medicine, Salt Lake City, UT 84132

Abstract

Photoreceptor degenerations initiated in rods or the retinal pigmented epithelium usually evoke secondary cone death and sensory deafferentation of the surviving neural retina. In the mature central nervous system, deafferentation evokes atrophy and connective re-patterning. It has been assumed that the neural retina does not remodel, and that it is a passive survivor. Screening of advanced stages of human and rodent retinal degenerations with computational molecular phenotyping has exposed a prolonged period of aggressive negative remodeling in which neurons migrate along aberrant glial columns and seals, restructuring the adult neural retina *(1).* Many neurons die, but survivors rewire the remnant inner plexiform layer (IPL), forming thousands of novel ectopic microneuromas in the remnant inner nuclear layer (INL). Bipolar and amacrine cells engage in new circuits that are most likely corruptive. Remodeling in human and rodent retinas emerges regardless of the molecular defects that initially trigger retinal degenerations. Although remodeling may constrain therapeutic intervals for molecular, cellular, or bionic rescue, the exposure of intrinsic retinal remodeling by the removal of sensory control in retinal degenerations suggests that neuronal organization in the normal retina may be more plastic than previously believed.

Index Entries: Retinitis pigmentosa; retinal dystrophies; plasticity, deafferentation; computational imaging; immunocytochemistry; amino acids.

Introduction

The retina is compartmentalized at the external limiting membrane into the distal transduction-competent outer limbs of rod and cone photoreceptors (the *sensory* retina) and the proximal synaptic-transmission competent inner limbs of photoreceptors and the rich array of neurons they drive (the *neural* retina). Retinal degenerations typically start in the sensory retina, eventually leading to complete deafferentation of the neural retina. For example, retinitis pigmentosa (RP) is a family of inherited retinal degenerations, with many variants arising with rhodopsin gene mutations

Received 2/19/03; Accepted 2/24/03.
* Author to whom all correspondence and reprint requests should be addressed. E-mail: robert.marc@hsc.utah.edu

(2). RP and related disorders, although initiated in rods, eventually impair cone vision. Clinical rescue of photoreceptors is still impossible, and cell transplants *(3,4)* and bionic implants *(5–7)* have been proffered as therapies to restore photic drive to the remnant neural retina. It is often asserted or assumed *(8,9)* that the neural retina is only minimally changed following photoreceptor loss, although data from human RP material suggest otherwise *(10).* Indeed, as soon as photoreceptors begin to malfunction in the *Pdeb6^{rd1}* mouse, bipolar cells and rod-targeted horizontal-cell axon terminals retract their dendrites *(11,12).* Defects in the cone pathway appear as neurite sprouting by both cones *(13)* and cone horizontal cells *(12).* Thus, the appearance of anomalous neurites in surviving rods and horizontal and amacrine cells of the human retina appears to be a common feature of retinal degenerations *(10).* Most—and especially autosomal—dominant retinal degenerations progress slowly, so it is difficult to say with confidence that remodeling is a general attribute, and even more difficult to evaluate the actual sequelae of remodeling over time. By screening an extensive library of human and aged natural, transgenic, and knockout rodent retinal degenerations with computational molecular phenotyping *(14,15)* and overlay electron microscopy *(16),* we have determined that remodeling is the general end stage of retinal degeneration, and that is it a complex, multicellular process involving all types of retinal neurons and glia *(1,17).*

Methods

Specimens

All specimens were acquired and processed as described in Jones et al. *(1).* Aldehyde-fixed human RP tissue was obtained from The Foundation Fighting Blindness Retina Donor Program. Animal tissues were harvested after intraperitoneal barbiturate or urethane anesthesia, followed by perfusion with or enucleation and immersion in buffered 2.5% glutaraldehyde/1% paraformaldehyde. Some were post-fixed in 1% buffered osmium tetroxide, and all were resin-embedded and processed for computational molecular phenotyping and electron microscopy *(14–16).* Specific models included: transgenic S334ter rats (truncated rhodopsin), transgenic P23H rats (mutated rhodopsin), RCS rats (natural RPE *mertk* defect), *Pde6b^{rd1}* mice (natural *pde6*β non-sense mutation), transgenic GHL mice (mutated rhodopsin), transgenic TG9N mice (RGS N-terminal fragment expression); *nr* mice (natural Purkinje-cell degeneration and rod degeneration), or mice (natural *chx10* homeobox gene null mutation), knockout *Chx10/p27^{Kip1}* mice (*p27^{Kip1}* knockout rescue model of *or*), *pcd* mice (natural Purkinje-cell degeneration with slow rod degeneration), *Prph2^{rd2}* (formerly rds) mice (natural peripherin2 defect); knockout *Rho*–/– mice (*Rho* knockout), and transgenic RhoΔCTA mice (truncated rhodopsin).

Computational Molecular Phenotyping

All samples thin sectioned into serial arrays *(18)* and probed *(14)* with IgGs targeting L-alanine, L-aspartate, L-glutamate, L-glutamine, glutathione, glycine, taurine, GABA (Signature Immunologics, Inc., Salt Lake City, UT), visualized as high-resolution (243 nm/pixel) images, mosaicked, and registered (PCI Geomatica V8.2 PCI Geomatics, Richmond Hill, Ontario, Canada) into image databases. Classifications using isodata clustering *(15),* theme-map generation, and analysis were performed by PCI Geomatica, and custom software written in IDL (Research Systems Inc., Boulder, CO). All images were prepared in Adobe Photoshop V7.01 (Adobe Systems Inc., San Jose, CA).

Electron Microscopy and Overlay Microscopy

Conventional transmission electron microscopy was performed as previously described *(16)* on 90-nm lead-stained sections on single-hole grids. Sections serial to the section reserved for electron microscopy were processed for computational phenotyping, and the optical

theme maps were registered to the ultrastructure as described here. Data were registered as described, and electron image theme maps were produced.

Modeling

Simple linear models of bipolar and amacrine-cell networks were generated in the Extend™ continuous systems modeling environment (Imagine That Inc., San Jose, CA) as previously published *(16),* using combinations of operational amplifiers and filters to mimic the linear impulse responses of typical bipolar cells *(19).* More than one hundred combinations of errors were modeled, representing the major classes of wiring defects.

Results

Computational molecular phenotyping transforms cell anatomical data into multidimensional molecular signatures that can be parsed by classification algorithms to formally classify all cells into the major neuronal types, subtypes, and, ultimately, natural classes *(15),* providing quantitative visualization as theme maps of somatic and neurite topologies. Unlike other immunocytochemical strategies, computational molecular phenotyping classifies all cells and tracks the fates of the major retinal-cell types and subtypes across different models and species with constant performance. The rodent models included degenerations associated with: transduction defects in rhodopsin (RhoΔCTA mouse, S334ter rat) or downstream elements (*Pde6b*^{rd1} mouse, TG9N mouse); protein absence (rhodopsin knockout rho$^{-/-}$ mouse); endoplasmic reticulum biosynthetic errors (GHL mouse, P23H rat); structural defects (*rd2* mouse), retinal pigment epithelium (RPE) phagocytosis defects (RCS rat); developmental hypocellularity defects (*chx10* and *chx10/P27* knockout mice), and natural neurodegeneration models of unknown mechanism (*nr* mouse, *pcd* mouse). The various molecular defects of these models influence the timing and coherence of cell death, resulting in different rates of disease progression and retinal remodeling. We first discovered global remodeling in the GHL mouse, a relatively slow rod degeneration model that exhibits progressive shortening of outer rod segments prior to rod death, during the first year of life *(20).* No major remodeling occurs in this phase, although rod circuitry may be subtly altered in early degeneration stages, as in the *rd* mouse. An unknown mechanism eventually leads to cone death *(21),* and remodeling of the neural retina begins between P200 and P345. By P500, however, massive remodeling has emerged, and we have found this pattern to be typical of many degeneration models, including advanced human RP (Table 1). The exceptions are the cone-sparing models in which remnant cones persist beneath the glial seal for extended periods of time. In the RCS rat, a natural model of retinal degeneration, a *mertk* gene RPE defect *(22)* progresses to photoreceptor death, remodeling onset by P270, and extensive remodeling by P645. As visualized in computational theme maps, all cells in the normal adult rat retina (Fig. 1A) computationally separate by isodata clustering into one of eight types (photoreceptor, bipolar, horizontal, amacrine, ganglion, Müller, RPE cells, and vascular endothelium) and selected subtypes (e.g., GABAergic and glycinergic amacrine cells). Global remodeling is characterized by the presence of columns of hypertrophic Müller glia, along with a dense layer of glial processes that seal the neural retina from the surviving RPE (Fig. 1B). This transformation is common to most advanced retinal degenerations, ranging from the slow GHL mouse to the moderate RCS rat and the rapid P23H-1 rat (Fig. 1C) and TG9N mouse models, as well as advanced human RP (Fig. 1D). Glial somas translocate throughout the remnant retina and neuron types migrate on glial surfaces, effecting repositionings of amacrine cells to both the distal glial seal and the remnant ganglion-cell layer (Fig. 1B), breaking the laminar organization of the retina. Neuronal migration is easily quantified by the appearance of glycinergic amacrine cells in the ganglion-cell layer. Glycinergic cells are normally excluded from the ganglion-cell layer,

Table 1
Remodeling in Retinal Degenerations

Species	HS	tRN	tRN	RN	MM	tMM	tMM	MM	MM	koMM	MM	MM	tMM	tMM
Gene defect	mixed	*rho*	*rho*	*mertk*	*pde6b*	*rho*	*rgs9*	?	*chx10*	$p27^{Kip1}$	Agtpbp1	prp2	rho	rho
Model	RP	S334ter	P23H	RCS	*rd1*	GHL	TG9N	*nr*	or	*chx10*(b)	*pcd*	rd2	rho−/−	rhoΔCTA
Specimens	20	9	12	7	9	8	19	3	3	1	2	1	4	8
Onset	?	P340	P372	P270	P610	P555	P160	P300	<P0	<P63	P321	>P151	>P365	>P541
Neurons														
Cell Death	+	+	+	+	+	+	+	o	+	+	o	o	o	o
strictures	+	+	+	+	+	+	+	+	+	+	o	o	o	o
dGlyACs/mm	2	4	6	12	2	6	35	2	(a)	5	o	o	o	o
fascicles	+	+	+	+	+	+	+	+	+	+	o	o	o	o
microneuromas	+	+	+	+	+	+	+	+	+	+	o	o	+	+
Glia														
Migration	+	+	+	+	+	+	+	+	+	+	o	o	o	o
Columns	+	+	+	+	+	+	+	+	+	+	+	o	o	o
Seals	+	+	+	+	+	+	+	+	o	o	+	+	+	+
Other														
VC invasion	?	+	+	+	+	+	+	+	+	+	o	o	o	o
RPE invasion	+	+	+	+	+4+	+	+	+	o	o	o	o	o	

+ present; o absent; ? undetermined; dGly ACs = displaced glycinergic amacrine cells; t = transgenic; ko = knockout; HS = *Homo sapiens;* RN *Rattus norvegicus;* MM *Mus musculus*. (a) Only isolated retinal patches survive in *chx10.* (b) The $p27^{Kip1}$ ko rescues hypocellularity in *chx10,* but also exhibits neuronal remodeling. From *(1).*

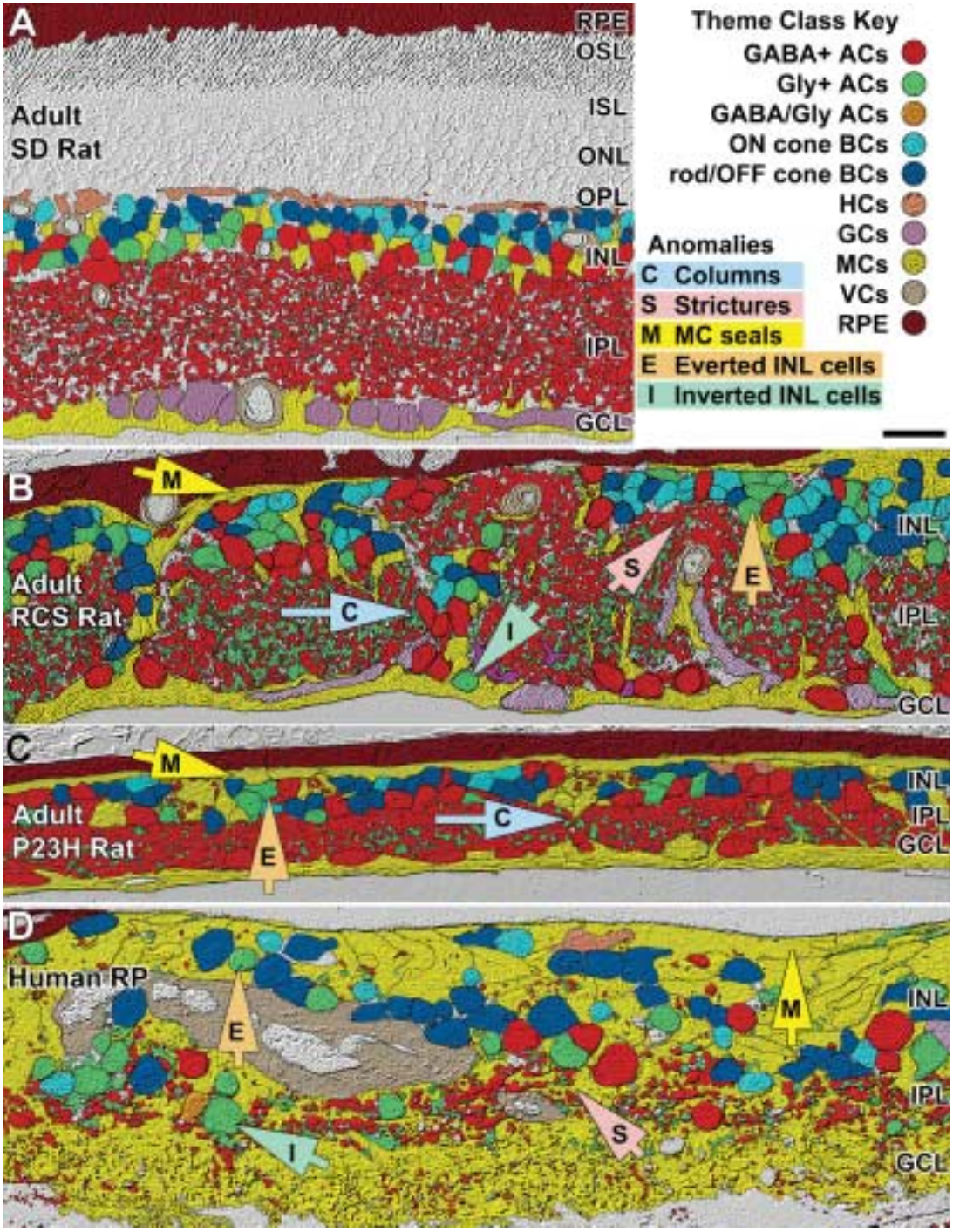

Fig. 1. Computational theme maps of **(A)** normal P700 Sprague-Dawley (SD) rat, **(B)** P900 RCS albino rat, **(C)** P372 P23H line 1 transgenic rat, and **(D)** human RP (Foundation Fighting Blindness accession #133-OD, 67 yo, female, advanced RP, simplex, fixed for 2.5 h post-mortem). In normal retina, cell layers are precisely defined. Remodeling clearly disrupts lamination through migration on Müller glia columns **(C)**, yielding eversion **(E)** of GABAergic and glycinergic amacrine cells to the distal Müller glial seal (M) and inversion of amacrine and bipolar cells (I) to the ganglion-cell layer. Glial hypertrophy and neuronal movement can be so extensive that the inner plexiform layer is segmented, distorted and forced through strictures (S) as small as 10 µm. From *(1),* with permission.

occurring at a frequency of <<0.001/mm. Advanced remodeling produces focal values of 2–35 cells/mm, a ≈10^3–10^4-fold increase in cell migration (Table 1). This misplacement is invisible to conventional histological assays. Cell death depletes all cell types, leading to thinning of the fragmented inner nuclear layer (INL) and loss of cells from the ganglion-cell layer. Cell loss is patchy, ranging from 25–50% in the INL of slow models. More than 90% of ganglion cells can be lost in fast, aggressive degenerations, such as the rat P23H-1 model *(23),* which can evoke such rapid neuronal death (Fig. 1C) that little migration evolves. In this model, many bipolar and amacrine cells die, and the ganglion-cell layer is largely acellular, except for remnant flattened neurons with molecular signatures of amacrine cells. Thus, these rodent models come to resemble the cell cohorts and topologies of advanced human RP retinas, in which long remodeling epochs can evoke even greater glial hypertrophy and neuronal loss (Fig. 1D).

Remodeling neurons also engage in the elaboration of new processes and synaptic complexes. New fascicles of ectopic neurites travel throughout the retina, apparently on glial surfaces, giving rise to as many as 30,000 new 20–100-µm diameter microneuromas in a given retina. Microneuromas are made of GABAergic and glycinergic amacrine-cell and glutamatergic bipolar-cell processes (Fig. 2A). Aberrant circuitries in microneuromas and the remodeled inner plexiform layer (IPL) include concatenated conventional (Fig. 2B), ribbon and multi-projection (Fig. 2C–G), and novel synaptic forms (Fig. 2H). Normal retinal bipolar cells drive target cells exclusively through fast, sustained vesicular glutamate release at ribbon synapses. Bipolar cells of remodeled retinas make extensive contacts in microneuromas and the inner plexiform layer, but their presynaptic forms are modified as i) numerous small ribbons capable of recruiting only a row or two of vesicles (Fig. 2F), ii) ribbon-free non-dyadic synapses (Fig. 2H), iii) somatodendritic (not shown) and iv) ribbon synapses onto amacrine-cell somas (Fig. 2C). Even bipolar-cell somas make ribbon synapses onto targets. Arguably, even with characteristic cytology and high vesicle content, the absence of synaptic ribbons compromises bipolar-cell identification, especially in remodeling. Thus, multichannel overlay and serial immunogold microscopy was performed to precisely define the molecular signatures of the profiles. The large ribbon-free presynaptic specializations in Fig. 2H are made by a cell with the unique signature of an ON-center cone bipolar cell (high glutamate, moderate glycine, low taurine, coded blue), and the targets are both GABAergic amacrine cells (coded orange). These presynaptic forms are not found in bipolar cells of the mature retina. Apparent bipolar-cell synapses also target other bipolar cells (Fig. 2C,D), representing re-entrant and cross-channel pathways, while amacrine cells make numerous novel multiprojection synapses (Fig. 2D), and both of these are absent from normal retina.

Remodeled retinas clearly contain wiring errors and synaptic forms unlike those of mature mammalian retina. If we imagine the successful restoration of light-driven input to the neural retina by cellular or bionic means, how do wiring errors influence signal processing? Cone and rod degeneration leave remnant circuits without high-gain glutamatergic drive (Fig. 3), and as new synapses impinge on remnant ON and OFF channels, respectively formed by depolarizing bipolar (BD) and amacrine cells (AD) and hyperpolarizing bipolar (BH) and amacrine cells (AH), they cannot simply insert into the fundamental synaptic architectures we have known for over three decades *(24).* Given the loss of photoreceptor inputs to the neural retina, *any* remodeling that restores glutamatergic input to bipolar cells must be corruptive, as re-entrant or cross-channel signaling from bipolar cells is the only known source of glutamatergic drive. Considering only the bipolar and amacrine-cell elements of the channels, ten single (Fig. 3A; Table 2) and 1,013 combinatorial errors can occur, and far more are possible if we include all other neuron types and all subclasses of bipolar cells *(25).* We modeled all major types of errors using complete network architectures *(16),* and determined that all single connective errors corrupt

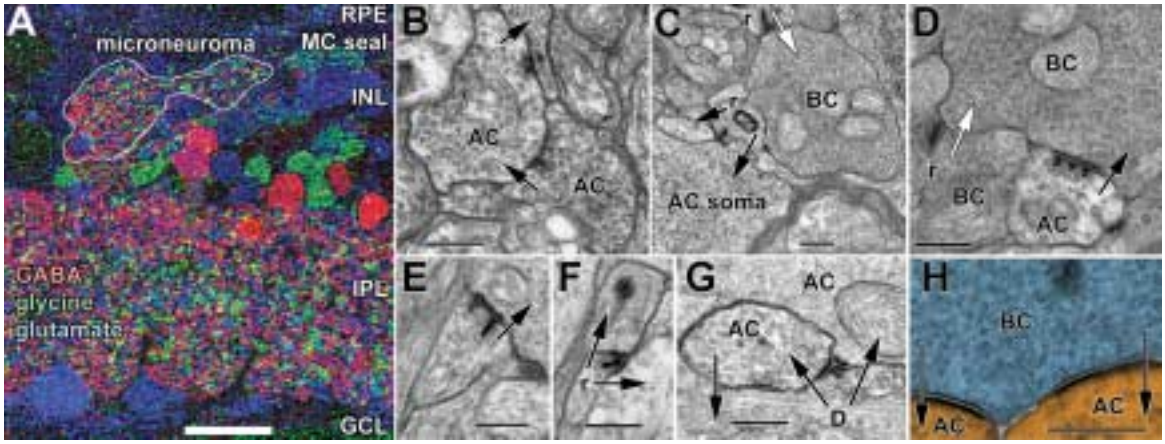

Fig. 2. Microneuromas and aberrant synaptic morphology. **(A)** GABA/glycine/glutamate → *rgb* mapping of RCS rat retina showing the emergence of new neuropil beneath the distal Müller cell (MC) seal. Microneuromas are tangles of GABAergic (red), glycinergic (green), and glutamatergic (blue) neurites. Scale = 20 μm. **(B)** Microneuroma amacrine → amacrine → target synapse chains. **(C)** Anomalous bipolar → amacrine-cell soma and bipolar → bipolar synapses. **(D)** Novel presynaptic multiprojection amacrine → bipolar and bipolar → bipolar cell contacts. **(E)** Multiprojection amacrine cell synapse mimicking bipolar cell ribbons. **(F)** Classic bipolar cell presynaptic dyad element in a process ≈ 100-nm diameter, with few vesicles. **(G)** Anomalous dyad-like synapse **(D)** with amacrine cell feedback. The presynaptic element contains few vesicles and resembles an amacrine-cell dendrite. **(H)** Electron imaging theme map of a large bipolar-cell terminal lacking ribbons, but making large conventional contacts onto amacrine-cell dendrites. The blue overlay denotes the signature of an ON-center cone bipolar cell; orange denotes GABAergic amacrine cells. Synaptic directions indicated by arrows; white arrows, bipolar → bipolar-cell contacts. Scale for all electron micrographs-200 nm. From *(1),* with permission.

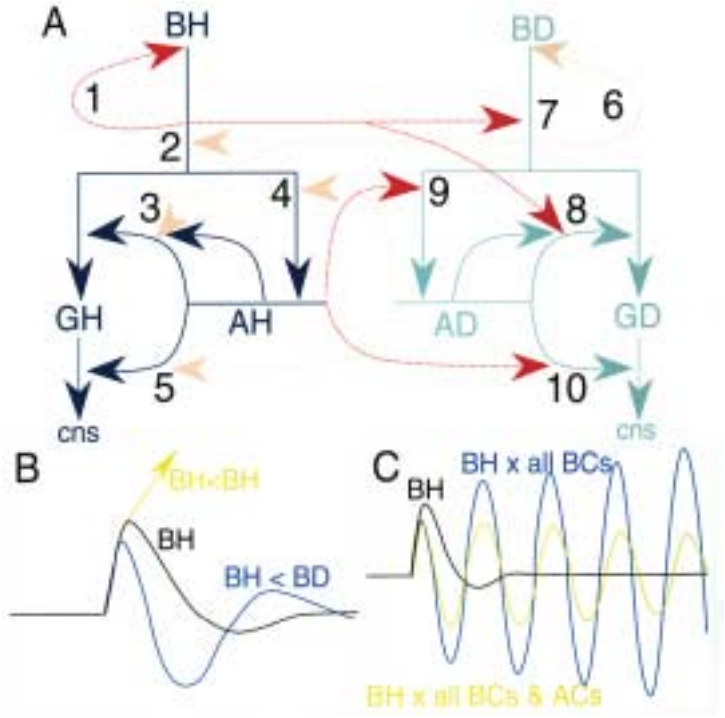

Fig. 3. Modeling of deafferented circuit corruption via cross-communication and reentrant excitation. **(A)** Deafferented ON channels are formed by depolarizing bipolar (BD), amacrine (AD), and ganglion-cell (GD) circuits shown as solid pale blue lines; deafferented OFF channels are formed by hyperpolarizing (BH), amacrine (AH) and ganglion cell (GH) circuits shown as dark blue solid lines. Ten single types of wiring errors (*see* Table 2) are shown as dotted lines; pale red lines indicate errors arising from ON channel cells; dark red lines arise from OFF channel cells. All bipolar cells are glutamatergic; all amacrine cells are GABAergic. **(B)** Modeled impulse responses of hyperpolarizing cone bipolar cell to brief "glutamate" excitation pulses (10 ms, dot) applied to all bipolar cells in normal (BH, black), single re-entrant (BH < BH, gold, error 1), and single cross-channel (BH-BD, cyan, error 2) circuits. Vertical axis, relative voltage; trace duration 0.5 s. **(C)** Modeled impulse responses in normal (BH, black), complete bipolar-cell cross-channel (BH × all BCs, cyan, errors 2,3,7,8), and complete neuronal cross-channel circuits (BH × all ACs and BCs 2,3,4,5,7,8,9,10), gold, errors 2). Vertical axis, relative voltage; trace duration 1 s. From *(17),* with permission.

Table 2
Types of Single Wiring Errors and Their Impacts on Bipolar-Cell Signaling

ID	Circuit	Definition	Effect on bipolar cell response
1	BH > BH	Reentrant KAr loop	BH step-function
2	BD > BH	Cross-channel KAr signal	BH transient oscillation
3	BD > AH	Cross-channel AMPAr signal	BH slowed
4	AD > BH	Cross-channel GABAr signal	BH slowed
5	AD > AH	Cross-channel GABAr signal	BH undershoot slightly larger
6	BD > BD	Reentrant mGluR6 loop	BD attenuated
7	BH > BD	Cross-channel mGluR6 signal	BD larger and slowed
8	BH > AD	Cross-channel AMPAr signal	BD slowed
9	AH > BD	Cross-channel GABAr signal	BD slowed
10	AH > AD	Cross-channel GABAr signal	BD undershoot slightly larger

encoding to variable degrees (Fig. 3B; Table 2). Re-entrant and cross-channel bipolar-cell signals seriously corrupt outputs in characteristic ways. BH > BH loops create positive feedback that forces persistent BH-step responses to any input, preventing proper spatiotemporal encoding (Fig. 3B), while BD > BD loops are self-attenuating as a result of sign-inverting mGluR6 transduction. BD > BH crossings shorten BH responses and make them briefly oscillatory (Fig. 3B), and BH > BD crossings greatly enhance and slow BD responses. However, multiple errors are even more likely, and most of these trigger resonant responses that preclude visual processing. If all bipolar cells engage in crossing synapses, outputs resonate without damping, and if all bipolar and amacrine cells cross circuits, oscillations damp slowly, on a scale of tens of seconds (Fig. 3C). Stable visual processing can only occur if all novel synapses exactly recapitulate normal wiring—which is clearly impossible—or if all crossings and re-entrant synapses occur with signal transfer weights that exactly counteract each other (statistically improbable).

Discussion

Retinal degenerations appear to have a common fate. Cone loss in most retinal degenerations appears to activate formation of glial columns and seals, cell migration, neuronal loss, and rewiring. This large-scale remodeling is similar to that triggered in retinal detachment *(26),* and appears to be a general retinal reaction to challenge. Rewiring indicates that remodeled retinas probably cannot process visual signals properly, even discounting the equally serious defects of topologic rearrangements and neuronal death. What triggers this profusion of new synapses, and how are partners found? Differential expression of protocadherin gene variants *(27)* have emerged as a plausible mechanism controlling interneuronal adhesion patterns, and changes in the expression of protocadherins, integrins, or for cell-adhesion proteins may evoke novel wiring patterns in remodeled retinas.

Deprivation or denervation can greatly alter the structures and natures of central sensory pathways by triggering atrophy of targeted neurons *(28)* and remodeling of corticothalamic connectivity *(29,30).* The retina, it turns out, is no different. Much of central nervous system (CNS) remodeling involves attempts of central neurons to recapture excitatory inputs, and we suspect that retinal remodeling is, similarly, a search by amacrine-cell and bipolar cells, particularly for excitatory inputs. This manifests itself as re-entrant oscillatory, but visually fictive, mechanisms. Recent physiological analyses of mouse postnatal retinal development indicate that retinal circuitry is shaped by post-

natal light history *(31)*. It is possible that retinal neurons normally retain the ability to rewire throughout life, and when challenged by deafferentation, the result of this rewiring is intrinsically negative and corruptive.

Retinal remodeling is a challenge for retinal transplant and implant strategies. The fibrotic Müller-cell seal invests the neural retina, and cannot be extricated. This requires the presence of direct cells into the retina, rather than into the hospitible subretinal space, and this carries the risk of cell fusion *(32)*. It is doubtful that transplantation can, in any way, retard remodeling, and may actually exacerbate it. The glial seal also renders the subretinal implant approach doubtful, as the glial investment cannot be overcome and the normal patterning of retinal cells on which such implants rely *(7,9)* is compromised. Global rewiring, anomalous circuits, neuronal death, and general disorder in retinal patterning also render most epiretinal implant schemes ineffective. Patients must be chosen very carefully to optimize the success of such methods.

Acknowledgment

This work was supported by the National Eye Institute (EY02576 RM).

References

1. Jones B.W., Watt C.B., Frederick J.M., Baehr W., Chen C.K., Levine E.M., et al. (2003) *J. Comp. Neurol.* **464,** 1–16.
2. http://www.sph.uth.tmc.edu/RetNet/
3. Young M.J., Ray J., Whiteley S.J.O., Klassen H., and Gage F.H. (2000) *Mol. Cell. Neurosci.* **16,** 197–205.
4. Coffey P.J., Girman S., Wang S.M., Hetherington L., Keegan D.J., Adamson P., et al. (2002) *Nature Neuroscience* **5,** 53–56.
5. Humayun M.S., de Juane E.J., Dagnelie G., Greenberg R.J., Propst R.H., and Phillips D.H. (1996) *Arch. Ophthalmol.* **114,** 40–46.
6. Chow A.Y. and Chow V.Y. (1997) *Neurosci. Lett.* **225,** 13–16.
7. Zrenner E., Gabel V.P., Haemmerie H., Hoefflinger B., and Shubert M. (1998) *Ophthalmic Res.* **30,** 197–198.
8. Scarlatis G. (2000) *MSJAMA* **283,** 2297.
9. Zrenner E. (2002) *Science* **295,** 1022–1025.
10. Fariss R.N., Li Z.-Y., and Milam A.H. (2000) *Am. J. Ophthalmol.* **129,** 215–223.
11. Strettoi E. and Pignatelli V. (2000) *Proc. Natl. Acad. Sci. USA* **97,** 11,020–11,025.
12. Strettoi E., Porciatti V., Falsini B., Pignatelli V., and Rossi C. (2002) *J. Neurosci.* **22,** 5492–5504.
13. Fei Y. (2002) *Mol. Vis.* **8,** 306–314.
14. Marc R.E., Murry R.F., and Basinger S.F. (1995) *J. Neurosci.* **15,** 5106–5129.
15. Marc R.E. and Jones B.W. (2002) *J. Neurosci.* **22,** 412–427.
16. Marc R.E. and Liu W. (2000) *J. Comp. Neurol.* **425,** 560–582.
17. Marc R.E., Jones B.W., Watt C.B., and Strettoi E. (2003) *Prog. Ret. Eye Res.* **22,** 607–655.
18. Marc R.E. (1999) *J. Comp. Neurol.* **407,** 47–64.
19. Naka K. (1977) *J. Neurophysiol.* **40,** 26–43.
20. Frederick J.M., Krasnoperova N.V., Hoffmann K., Church–Kopish J., Rüther K., Howes K., Lem J., and Baehr W. (2001) *Investig. Ophthalmol. Vis. Sci.* **42,** 826–833.
21. Mohand-Said S., Deudon-Combe A., Hicks D., Simonutti M., Forster V., Fintz A.-C., et al. (1998) *Proc. Natl. Acad. Sci. USA* **95,** 8357–8362.
22. D'Cruz P.M., Yasumura D., Weir J., Matthes M.T., Abderrahim H., LaVail M.M., and Vollrath D. (2000) *Hum. Mol. Genet.* **9,** 645–651.
23. Machida S., Kondo M., Jamison J.A., Khan N.W., Kononen L.T., Sugawara T., Bush R.A., and Sieving P.A. (2000) *Investig. Ophthalmol. Vis. Sci.* **41,** 3200–3208.
24. Dowling J.E. (1968) *Proc. R. Soc. Lond. Sec. B. Biol. Sci.* **158,** 232–252.
25. Euler T., Schneider H., and Wässle H. (1996) *J. Neurosci.* **16,** 2934–2944.
26. Lewis G.P., Charteris D.G., Sethi C.S., and Fisher S.K. (2002) *Eye* **16,** 375–387.
27. Tasic B., Nabholz C.E., Baldwin K.K., Kim Y., Rueckert E.H., Ribich S.A., et al. (2002) *Molecular Cell* **10,** 21–33.
28. Von Noorden G.K. and Crawford M.L.J. (1978) *Investig. Ophthalmol. Vis. Sci.* **17,** 762–768.
29. Buonomano D.V. and Merzenich M.M. (1998) *Annu. Rev. Neurosci.* **21,** 149–186.
30. Jones E.G. and Pons T.P. (1998) *Science* **282,** 1121–1125.
31. Tian N. and Copenhagen D.R. (2001) *Neuron* **32,** 439–449.
32. Terada N., Hamazaki T., Oka M., Hoki M., Mastalerz D.M., Nakano Y., et al. (2002) *Nature* **16,** 542–545.